


Research Article

The Potential Scattering Model for Oil Palm Phenology Based on Spaceborne X-, C-, and L-Band Polarimetric SAR Imaging

Soni Darmawan ¹, Ita Carolita,² Rika Hernawati ¹, Dede Dirgahayu,² Agustan ³,
Didin Agustian Permadi,¹ Dewi Kania Sari ¹, Widya Suryadini,¹ Dhimas Wiratmoko,⁴
and Yohanes Kunto¹

¹Institut Teknologi Nasional Bandung (ITENAS), PKH. Mustofa 23. Bandung 40124, Indonesia

²Remote Sensing Applications Center of National Institute of Aeronautics and Space (LAPAN), Kalisari 8, Pekayon, Pasar Rebo, East Jakarta 13710, Indonesia

³Agency for the Assessment and Application of Technology (BPPT), M.H Thamrin 8 Jakarta 10340, Indonesia

⁴Indonesian Oil Palm Research Institute, Brigjen Katamso 51, Medan 20158, Indonesia

Correspondence should be addressed to Soni Darmawan; soni_darmawan@itenas.ac.id

Received 27 November 2020; Revised 20 January 2021; Accepted 7 February 2021; Published 8 March 2021

Academic Editor: Zhenxing Zhang

Copyright © 2021 Soni Darmawan et al. This is an open access article distributed under the Creative Commons Attribution License, which permits unrestricted use, distribution, and reproduction in any medium, provided the original work is properly cited.

Information about oil palm phenology is required for oil palm plantation management, but using spaceborne polarimetric radar imagery remains challenging. However, spaceborne polarimetric radar on X-, C-, and L-band is promising on structure vegetation and cloud area. This study investigates the scattering model of oil palm phenology based on spaceborne X-, C-, and L-band polarimetric Synthetic Aperture Radar (SAR) imaging. The X-, C-, and L-band polarimetric SAR are derived from spaceborne of TerraSAR-X, Sentinel-1A, and ALOS PALSAR 2. Study area is located in oil palm plantations, Asahan District, North Sumatra, Indonesia. The methodology includes data collection, preprocessing, radiometric calibration, speckle filtering, terrain correction, extraction of scattering value, and development of scattering model of oil palm phenology. The results showed different scattering characteristics for the X-, C-, and L-band polarimetric SAR of oil palm for age and found the potential of the scattering model for oil palm phenology based on the X-band on HH polarization that showed a nonlinear model with $R^2 = 0.65$. The C-band on VH and VV polarization showed a nonlinear model with $R^2 = 0.56$ and $R^2 = 0.89$. The L-band on HV and HH polarization showed a logarithmic model with $R^2 = 0.50$ and $R^2 = 0.51$. In this case, the most potential of the scattering model of oil palm phenology based on R^2 is using C-band on VV polarization. However, the scattering model based on X-, C-, and L-band is potentially to be used and applied to identify the phenology of oil palm in Indonesia, which is the main parameter in yield estimation. For the future phenology model needs to improve accuracy by integrating multisensors, including different wavelengths on optical and microwave sensors and more in situ data.

1. Introduction

Oil palm (*Elaeis guineensis*) is a palm tree that is generally planted in Southeast Asia, particularly in Malaysia, Indonesia, and Thailand. Oil palm can produce cooking oil, mechanical oil, and fuel, widely utilized in daily life and industry [1, 2]. Oil palm obtained from seeds or portions in a hard mesocarp shell produces around 80% saturated fat that can be utilized as a raw material for the production of soap, cleansers, and other substances in the oleochemical

industry [3–5]. Oil palm has an exceptional potential to be used as a biofuel in the future [6]. High yields and low production costs from oil palm are the reasons that encourage commercial plantation companies to develop oil palm trees for a considerable scope [7]. Because of expanding worldwide interest for nourishment and fuel, oil palm cultivation has been extended exponentially [8], and nowadays, oil palm is one of the most consumed vegetable oils in the world [9].

Southeast Asia has the ideal condition for oil palm cultivation because it needs the moist equatorial condition [10].

Oil palm is adapting to the tropical atmosphere with a high precipitation rate, high intensity of global radiation, and warm temperature of 24–32°C [11]. The regular dry season in the tropical areas could significantly reduce oil palm yields [3]. The oil palms are generally planted in triangular patterns with a nine-meter interplanting distance (see Figure 1), following an industry standard to maximize yield with optimal sunlight penetration [3]. A planting density of 130–140 palms for each is the general practice. However, it varies according to the planting conditions and oil palm breed type [9, 12, 13]. Terrace planting usually facilitates a countermeasure to run off water and maximizing planting density in hilly areas [14].

Oil palm plantations are planted per block so that all plants in each block have a uniform age. The age of oil palm is the main parameter in yield estimation. Oil palm age is one of the significant variables affecting the production of fruit bunches [3, 10]. Age information of oil palm is a good indicator of yield prediction as it influences the quality and quantity of the fresh fruit bunches [16]. Besides, age information is essential to precision agriculture to recognize anomalies among oil palms inside a specific age group to plan counteractive management practices and optimize management resources [10, 17]. In other cases, oil palm age information is required for the tax estimation, replanting time, and identification of oil palm diseases [15]. Organization or plantation management favors such useful data for maximizing oil palm yield, one of the most important influencing benefits [10]. According to Tan et al. [10], collecting age information on oil palm trees is time-consuming and costly, particularly on a large or regional scale. The age of oil palm growth affects the physical and environment of the oil palm plantation itself. According to Tan et al. [10] and Chemura et al. [16], canopy height and size of oil palms have a strong correlation with age.

Spaceborne technology has been commonly applied in the agriculture and forestry sectors. These technologies are proven to provide a precise, affordable, and efficient solution for agricultural and forestry planning, monitoring, and management [18]. According to Henderson and Lewis [19], although sensors in the optical range of the electromagnetic spectrum have gotten the best consideration and have widely used, considerable effort has been invested into the utilization of radar sensors. Microwave sensors have become a promising technology in the application of remote sensing due to their cloud penetration ability and their capability to obtain data in all-weather day-night conditions. The microwave sensor also relies on its internal energy source, unlike the optical sensors, which rely on sunlight's external energy source. Scatter radar is very sensitive to the dielectric properties (soil moisture and vegetation) and attributes of the geometric conditions (surface roughness) of objects on the surface of Earth [20].

Many regions in the world (e.g., areas covered by clouds and lacking light), radar is the only sensor that can reliably provide consistent and periodic data. A radar sensor can obtain information in the electromagnetic spectrum bands K (1.1–1.7 cm), X (2.4–3.8 cm), C (3.8–7.5 cm), L (15–30 cm), and P (30–100 cm) [20], with the polarization of

Horizontal to Horizontal (HH), Vertical to Vertical (VV), Horizontal to Vertical (HV), or Vertical to Horizontal (VH), which have varying ranges and azimuth resolutions [21]. Each of these wavelengths has a unique characteristic related to the reflection from forest stands [22]. The X-band interacts with leaves and canopy cover surfaces; hence, it is very suited for information on the tree canopy surface layer [23]. The C-band can penetrate through the leaves and spread to small branches and other underlying objects [24]. The L-band, which has a higher penetration capability, can penetrate the surface layer and spread to the stems and main branches [25, 26]. The P-band has the highest penetration capability and can penetrate the canopy covers [27].

Many studies developed the model of oil palm phenology derived from scattering characteristics and any parameter, such as derived from biomass [27], leaf area index (LAI) [10, 17], height tree and tree diameter [10], crown projection area (CPA) [16], scattering [28], NDVI [10, 17, 29–31], and spectral band [10, 17, 28, 32]. However, to our best knowledge, information about phenology based on spaceborne X-, C-, and L-band polarimetric SAR has been limited and fragmented in Indonesia. In this study, we pioneered to investigate the scattering model of oil palm phenology in Indonesia based on spaceborne X-, C-, and L-band polarimetric SAR simultaneously.

2. Materials and Methods

2.1. Study Area. Study area in Asahan Regency, North Sumatra, Indonesia. This regency has the capital of Kisaran City and covers an area of 3702.97 km². A part of Asahan regency was selected as the study area, which is an oil palm plantation area located in Hessa Plantation, Simpang Empat, Asahan Regency, 2.98° east longitude and 99.67° north latitude and 2.92° east longitude and 99.75° north latitude (Figure 2).

The Asahan Regency is in the central part of the North Sumatra Province eastern coast. The district is mainly agricultural, and the primary land uses are oil palm and rubber plantations inland, with coconut groves and aquaculture ponds by the sea [33]. The first Indonesian oil palm plantation was founded in Asahan [34]. In 1911 during the Dutch colonial era, a Belgian company opened the first commercial oil palm plantation [35], and Asahan was a pioneer in the East Coast area of Sumatra [34, 36]. The large plantation area owned by many private companies and the state-owned Perkebunan Nusantara Company contributes a great deal to most Asahan citizens' economic needs. The plasma plantation scheme is owned by a smallholder whose management is supported by the company (as a central plantation) [34].

Asahan District has a factory capacity of 50 tons of fresh fruit bunch (FFB) per hour [37]. According to Budidarsono et al. [38], on the eastern coast of Sumatra, oil palm production (CPO) increased drastically. The area of the first farm, which was built in 1910–1914, was 2620 ha. The location biophysics is suitable for oil palm growing, with high rainfall (minimum 1600 mm/year) and a tropical climate within 10° of the equator. Land and labor, the most significant inputs, were available [38].

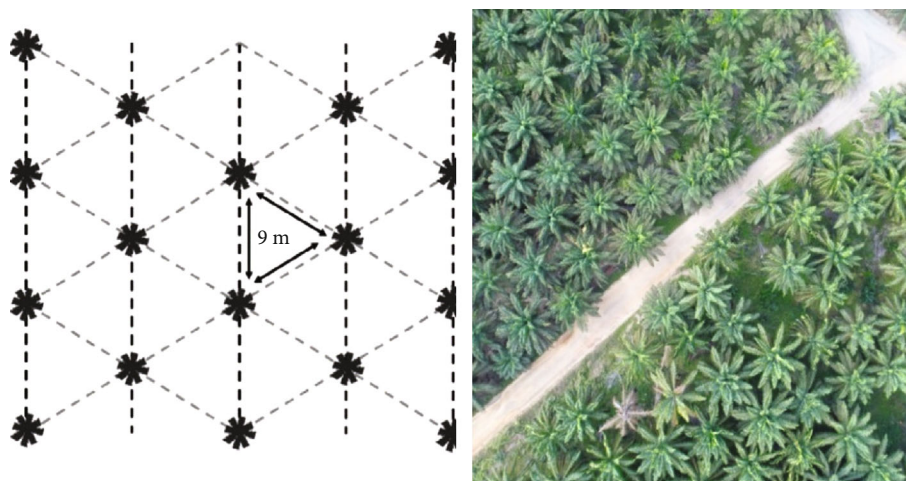


FIGURE 1: The oil palms planted in triangular patterns (source: [9, 15]).

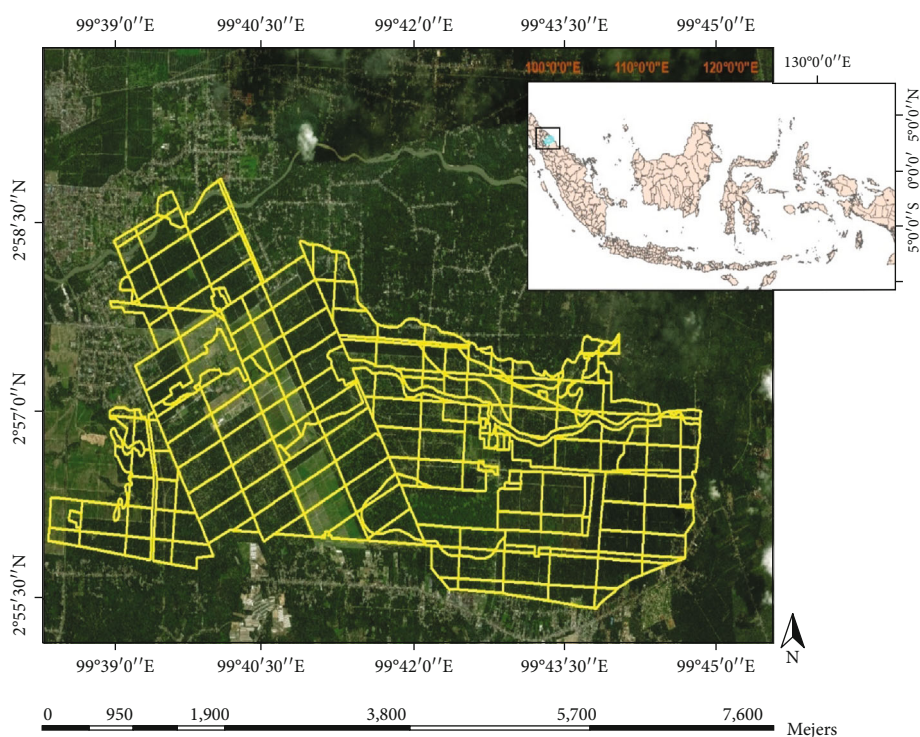


FIGURE 2: Study Area in Asahan Regency, North Sumatra, Indonesia.

2.2. Methodology. The methodology includes data collection, preprocessing, radiometric calibration, speckle filtering, terrain correction, extracting scattering value, and development scattering model based on spaceborne X-, C-, and L-band polarimetric SAR (Figure 3).

2.2.1. Data Collection. Collecting of variety polarimetric SAR imaging, including TerraSAR-X (X-band), Sentinel-1A (C-band), and ALOS PALSAR 2 (L-band) (Figure 4). TerraSAR-X and ALOS PALSAR-2 data were obtained from the National Institute of Aeronautics and Space-Indonesia (LAPAN), while Sentinel-1A data were collected from the

European Space Agency (ESA) Copernicus. The details of the SAR imaging are presented in Table 1.

The topography elevation data were derived from Shuttle Radar Topographic Mission (SRTM), which has a spatial resolution of around 90 meters, and were processed by the National Aeronautics and Space Administration (NASA) and the United States Geological Survey (USGS). The data were projected in a geographic (Lat/Lon) projection, with the WGS84 horizontal datum. Field data collection was conducted in 2020 that collected planting age blocks of oil palm and some photograph in the study area (Figures 5 and 6). In this study area, we used 174 blocks, which represent 11 varieties of oil palm age from 0 to 25 years. This planting age

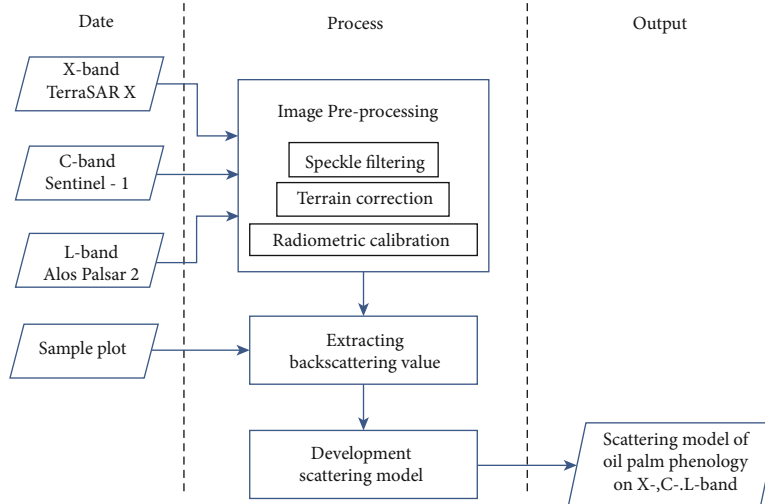


FIGURE 3: Methodology.

block data is used as a boundary in taking the region of interest (ROI) based on the scattering value with totally around 44,000 pixels.

2.2.2. Preprocessing

(1) *Speckle Filtering.* SAR imaging interpretation and classification principal problem is the speckle effect caused by wave coherent interference reflected from many primary scatterers [39]. Speckle appears in SAR imaging as granular noise due to waves interference reflected from many basic scatterers [40]. Speckle filtering is a procedure to increase image quality by reducing speckle. The enhanced Lee filter with a window size of 7×7 has been chosen in this study to minimize speckle effect on the images [41, 42], also to remove noise in the edge and high contrast area [40] without loss of information [43], because previous research showed reduction in speckles on SAR data using the Lee Filter before extracting the scattering value [24]. According to Lee et al., this algorithm is the best algorithm for segmentation crop filed purpose [40].

(2) *Terrain Correction.* The preprocessed image was also terrain correction to eliminate the distortion introduced by the topographical variations. The purpose of terrain correction for SAR imaging is to minimize the SAR geometry effects (foreshortening, layover, and shadow) towards radar images [24]. The Shuttle Radar Topography Mission (SRTM) was used as the Digital Elevation Model (DEM) to provide height information [44] using Range-Doppler Terrain Correction [24]. The geometric corrections were performed on all SAR (X-, C-, and L-band) data of the study area. All images were rectified, and the data were projected in geographic (Lat/-Long) projection, with the WGS84 datum.

(3) *Radiometric Calibration.* Calibration of the scattering values is necessary for the intercomparison of radar images acquired with different sensors or images obtained by the same sensor if acquired in different modes or processed with

different processors [45]. Radiometric calibration resulting in sigma naught (σ°) [45].

The radiometric calibration process for X-band first calculated the radar brightness β°_{dB} (beta zero, as contained in dB) derived from the polarization-specific calibration factor k_S (in equation (1)) and converted from digital numbers (DN) to sigma naught (σ°) using equation (2) [39, 46]:

$$\beta^\circ_{dB} = 10 \times \log_{10}(K_S DN^2). \quad (1)$$

The final radiometric calibration was performed by calculating sigma naught (σ°) using

$$\sigma^\circ = \beta^\circ_{dB} + \log_{10}(\sin \theta_{loc}). \quad (2)$$

where θ_{loc} , the local incident angle image, is defined for the four scenes' angle position, based on 2D interpolation across the performed image dimensions. The interpolation method applied is based on Delaunay's triangulation of data using the Qhull algorithm [47]. In conclusion, the local incident image has the same dimensions as the scene image and produces specific information about each pixel's local incident angle [39].

While the scattering value of the C-band is transforming the gamma-calibrated scattering coefficient [48], the C-band product uses a radiometric calibration look-up table (LUT) to do the calibration [49]. The essential conversion of amplitude to DN and from DN to sigma naught was done automatically on SNAP, and once the sigma naught values were obtained [41, 50], the computation of scattering (σ°_{dB}) can be performed in

$$\sigma^\circ_{dB} = 10 \cdot \log_{10}[\gamma_i], \quad (3)$$

where γ_i is the gamma-calibrated scattering coefficient of the C-band [48].

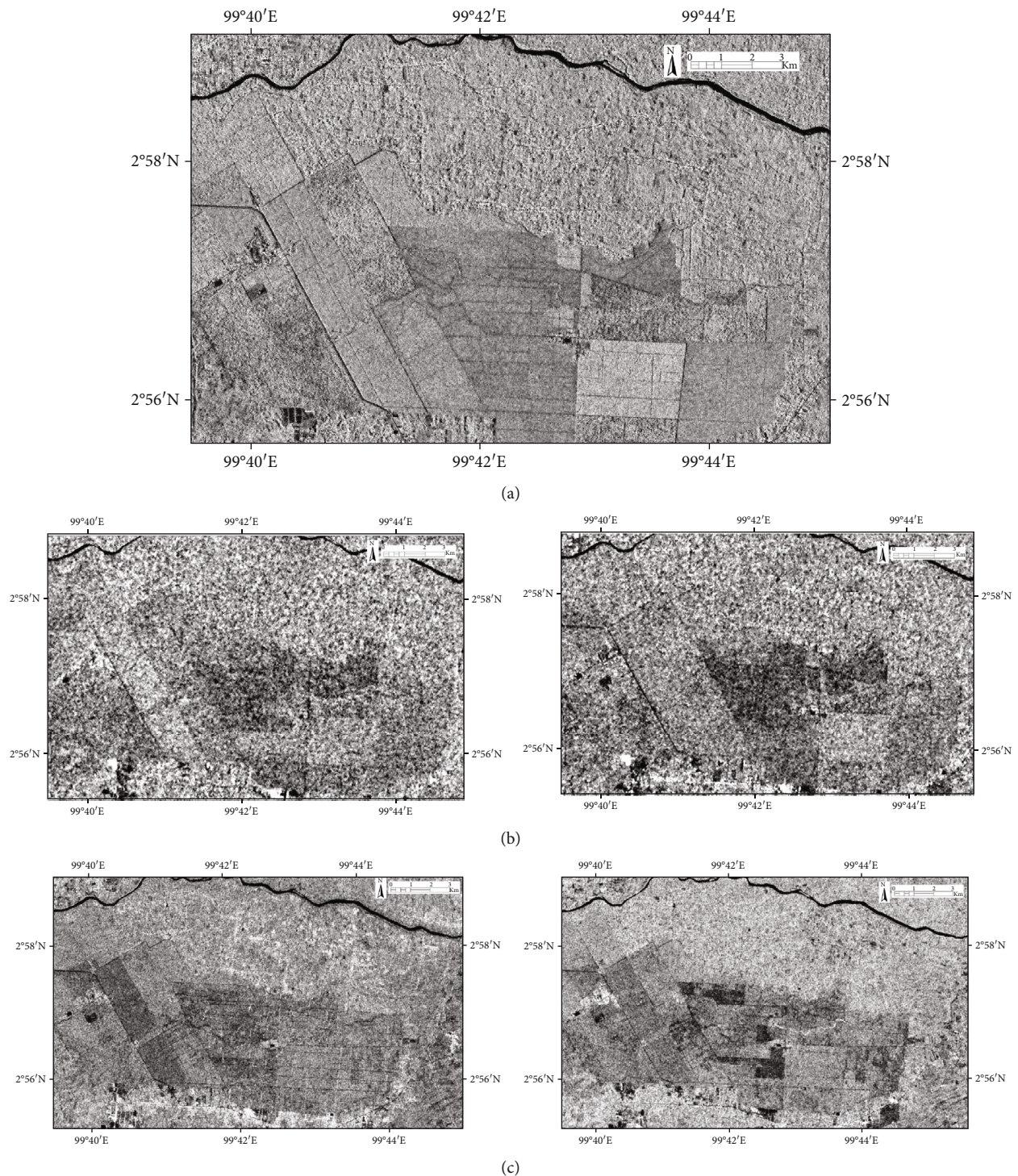


FIGURE 4: SAR imaging on TerraSAR-X on HH (a), Sentinel-1 on VV and VH (b), and ALOS PALSAR on HH and HV (c).

The L-band was built on a 16-bit data type, and all pixels have digital numbers (DN) ranging from 0 to 65,535 [41]. The DN has to be converted to scattering (i.e., the reflected radar signals) recognized as Normalized Radar Cross Section (NRCS) and expressed in σ° in decibels (dB) [41]. The conversion of HH (DN_{HH}) and HV (DN_{HV}) scattering intensities into NRCS (that is σ°_{HH} and σ°_{HV}) [28, 51] was based

on Shimada's study [51] shown in

$$\sigma^\circ_{HH} \text{ (dB)} = 10 \times \log_{10}(DN_{HH}^2) - CF, \quad (4)$$

$$\sigma^\circ_{HV} \text{ (dB)} = 10 \times \log_{10}(DN_{HV}^2) - CF, \quad (5)$$

where σ° is the scattering coefficient and CF is the calibration

TABLE 1: The characteristics of SAR data.

Sensor	TerraSAR-X	Sentinel-1A	ALOS PALSAR-2
Wavelength	X-band $\lambda = 3.1$ cm	C-band $\lambda = 5.6$ cm	L-band $\lambda = 23.5$ cm
Frequency	8-12 GHz	4-8 GHz	1-2 GHz
Polarization	Single HH	Dual VV/VH	Dual HH/HV
Resolution	Stripmap: 3×3 m	Interferometric Wide Swath (IW): 5×20 m	Stripmap: 3-10 m
Frame size	Stripmap: 50×30 km	IW: 250 km	Stripmap: $55 \times 70 - 70 \times 70$ km
Temporal	11 days	12 days	14 days
Date of acquisition	29 August 2017	15 July 2018	17 January 2015
Incidence angle range	28.7°	39°	34.9°

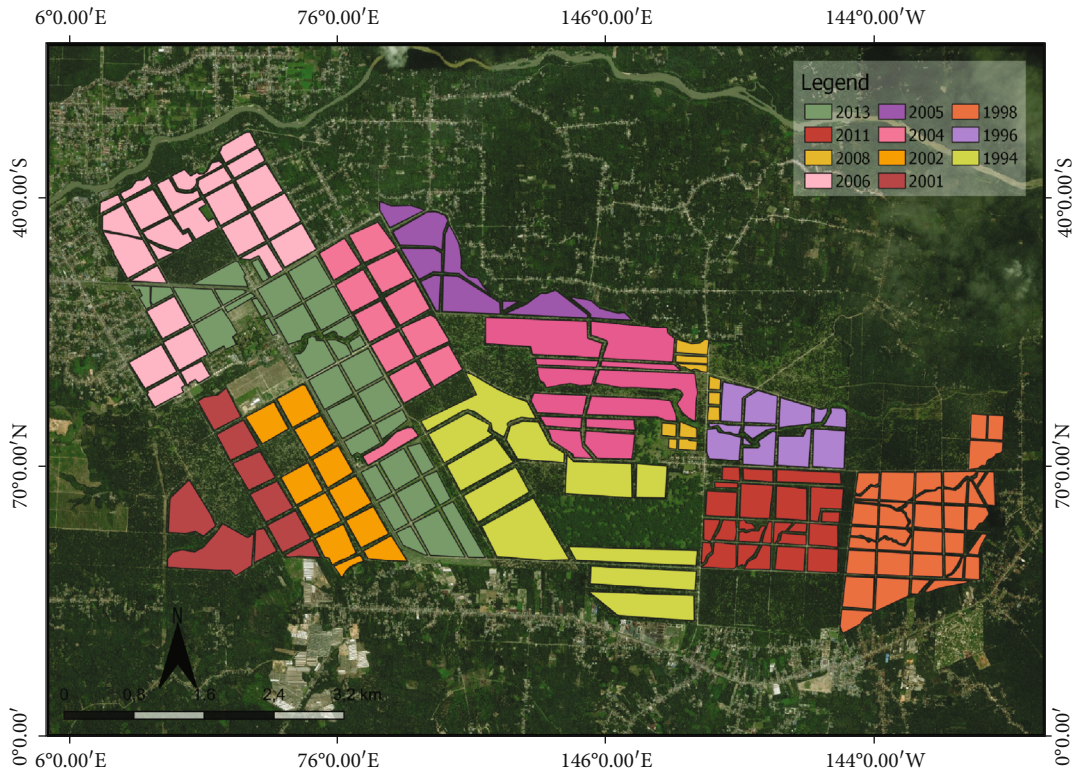


FIGURE 5: The planting age blocks of oil palm in the study area.

factor. The CF is dependent on the processing date. In this study, CF is equal to -83.0 both for HH and HV [28].

2.2.3. Extracting Scattering Characteristic. We created a region of interest (ROI) for area sampling; also the ROI was calculated to determine the scattering characteristics of X-, C-, and L-band polarimetric SAR imaging with the age of the oil palm in the forms of mean and standard deviation values using the algorithm as follows (equation (6) and (7)) [52]:

$$\bar{x} = \frac{\sum_{j=1}^n x_j}{n}, \quad (6)$$

$$s^2 = \frac{\sum_{j=1}^n (x_j - \bar{x})^2}{n - 1}, \quad (7)$$

where n is the number of samples taken, x_i is the sample value, \bar{x} is the average of the samples, and s is the standard deviation.

2.2.4. The Development of Scattering Model. We analyzed the relationship between the scattering value of SAR imaging polarization (X-band on HH, C-band on VV and VH, and L-band on HH and HV) and the age of oil palm plantation. The scattering response from oil palm areas depends on the structure and density of the oil palms. All oil palm ranges, and even under those circumstances, the various structures, and densities have different scattering patterns and textures at various wavelengths [28]. Analyzing the relationship between scattering and age is using the Pearson correlation coefficient (equation (8)). Pearson's method assumed that if the coefficient is similar to one, it implies a strong correlation



FIGURE 6: Oil palm age in study area.

between the two variables [53].

$$\sqrt{R^2} = r = \frac{\sum (X_i - \bar{X})(Y_i - \bar{Y})}{\left[\sum (X_i - \bar{X})^2 \sum (Y_i - \bar{Y})^2 \right]^{1/2}}, \quad (8)$$

where \bar{X} is the mean of the X variable and \bar{Y} is the mean of the Y variable. In this study, the first variable is the oil palm age, and the second variable is scattering polarization value. The coefficient of determination (R^2) is an indication of the regression model [54]. The R^2 value will show the percentage of variation as a regression model variable [55]. Several methods have been proposed to interpret the correlation coefficient into descriptors like “weak,” “moderate,” or “strong” relationship [56].

3. Results

The X-, C-, and L-band polarimetric SAR imaging was filtered using the Lee filter for each polarization. The scattering model of oil palm phenology was based on an empirical model derived from the relationship between oil palm age and scattering value of X-, C-, and L-band SAR imaging. In this study, ranges of oil palm age were divided for five years: 0-5, 5-10, 10-15, 15-20, and 20-25.

3.1. The Scattering Model of Oil Palm Phenology Based on X-Band. The scattering model of oil palm phenology was based on X-band with HH polarization. The value starts at the age of 0-5 years around -6.8 dB, of 5-10 years around -5.7 dB, of 10-15 years around -5 dB, and of 20-25 years around -6.4 dB (Figure 7). On HH polarization, the scattering model has nonlinear regression on $y = -0.0114x^2 + 0.2741x - 7.2823$ with $R^2 = 0.65$ (Figure 7).

3.2. The Scattering Model of Oil Palm Phenology Based on C-Band. The scattering model of oil palm plantation was based on C-band with VH and VV polarization. On VH polarization, the value starts in the age of 0-5 years around -14 dB,

age of 5-10 years around -15 dB, age of 10-15 years around -14 dB, age of 15-20 years around -15 dB, and age of 20-25 years around -16 dB (Figure 8(a)). On VH polarization, the scattering model has nonlinear regression $y = -0.0055x^2 + 0.1248x - 15.785$ with $R^2 = 0.56$ (Figure 8(a)).

On VV polarization, the value starts at the age of 0-5 years around -7.8 dB, at the age of 5-10 years around -7.4 dB, at the age of 10-15 years around -6.5 dB, at the age of 15-20 years around -7.4 dB, and at the age of 20-25 years around -8.0 dB (Figure 8(b)). On VV polarization, the scattering model has nonlinear regression $y = -0.0117x^2 + 0.3006x - 8.9534$ with $R^2 = 0.89$ (Figure 8(b)).

3.3. The Scattering Model of Oil Palm Phenology Based on L-Band. The scattering model of oil palm plantation based on L-band with HH and HV polarization. On HH polarization, the value starts at the age of 0-5 years around -12.6 dB, at the age of 5-10 years around -11 dB, at the age of 10-15 years around -11.3 dB, at the age of 15-20 years around -11.5 dB, and at the age of 20-25 years around -11.9 dB (Figure 9(a)). The scattering model has logarithmic regression $y = 0.5293 \ln(x) - 12.616$ with $R^2 = 0.51$ (Figure 9(a)).

On HV polarization, the value starts at the age of 0-5 years around -22 dB, at the age of 5-10 years around -18 dB, at the age of 10-15 years around -19 dB, at the age of 15-20 years around -18.9 dB, and at the age of 20-25 years around -18.5 dB (Figure 9(b)). The scattering model has logarithmic regression $y = 1.1555 \ln(x) - 21.815$ with $R^2 = 0.50$ (Figure 9(b)).

4. Discussion

Two significant characteristic categories determine the SAR scattering values are the sensor and the target characteristics [57]. The sensor category includes the frequency/wavelength of the SAR, the polarization of the transmitted and received SAR signal, the incident angle of the ground-interacting radar beam, and the sensor looking position [57]. According to Henderson and Lewis [19], the target characteristic

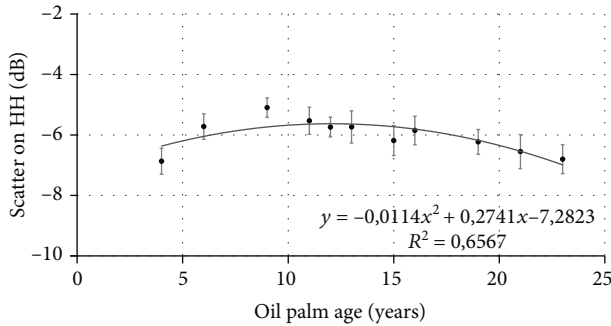


FIGURE 7: Scattering model of oil palm phenology on X-band with HH polarization.

influence varied with (1) vegetation type, (2) stand structure, and (3) canopy composition.

4.1. Characteristics Age of Oil Palm Based on SAR Imaging.

The scattering characteristics of the forest vegetation are influenced by the thickness of the volume, density of the component particles (or scatters), size distribution of the component particles, shape distribution of the component particles, orientation distribution of the component particles, and dielectric properties of the component particles [58]. It is essential to know the polarization from which the SAR image obtained because signals at different polarizations interact differently with objects on the ground, which affects the brightness of the radar recorded in a particular polarization channel [59]. For simplicity, it is assumed that a natural scene can be described as a combination of three types of scatterers: (1) rough surface scatterers, (2) double-bounce scatterers, and (3) volume scatterers [60].

4.1.1. On the X-Band. The scattering characteristics of the oil palm at the X-band of the young oil palm have the lowest scattering value as seen in Figure 10 of the 4-year-old histogram which is caused by rough surface scatters. The mature oil palm has a higher scattering value as seen in Figure 10 on the 6 to 15-year-old histogram which is caused by double-bounce scattering. The old oil palm has a lower scattering value as seen in Figure 10 of the 16 to 23-year-old histogram which is caused by volume scatters.

According to Martinis and Rieke [61], adopting the X-band, canopy attenuation, volume, and surface scattering from the top layer of the forest canopy is generally higher [62] because the X-band is sensitive to canopy surface scattering [63]. Hence, the same canopy surface seems rough for X-band wavelength causing high scattering values [64]. According to Rosenqvist [65], the X-band instrument clear relationship between canopy growth area and threshold ambiguity for trees.

4.1.2. On the C-Band. The scattering characteristics of oil palm at the C-band on VV and VH polarization on the young oil palm have the lowest scattering value as seen in Figures 11 and 12 on the histogram for 2 to 4-year-old histogram which is caused by rough surface scattering. The mature oil palm has a higher scattering value as seen in Figures 11 and 12 of the 7 to 14-year-old histogram which is caused by double-

bounce scattering. The old oil palm has a lower scattering value as seen in Figures 11 and 12 of the 17 to 21-year-old histogram which is caused by volume scatters.

According to Carolita et al. [15], increase and decrease in the scattering value occur because at the planting new age of trees height was relatively low and the size of the canopy is still small when the tree reached into productive age, the scattering value will rise because of the difference in the height of tree and soil. C-band data has a short wavelength, causing the scattering values for canopy density to become smaller. According to Teng et al. [6], there was also a significant contribution from the trunks to the surface volume scattering component, although this was not the dominant component. Also, at the shorter C-band wavelength, volume scattering can occur within the canopies of lower or sparse vegetation types, such as bushes, shrubs, or crops. According to Rignot et al. [66], radar signals were expected to be dominantly scattered by the foliage and the top branches and twigs of the canopy at the C-band.

4.1.3. On the L-Band. The scattering characteristics of oil palm at the L-band on HH and HV polarization on the young oil palm have the lowest scattering value as seen in Figures 13 and 14 on the 5-year-old histogram which is caused by in surface scattering. The mature oil palm has a higher scattering value as seen in Figures 13 and 14 of the 7 to 14-year-old histogram which is caused by double-bounce scattering. The old oil palm has a lower scattering value, as seen in Figures 13 and 14 of the 16 to 24-year-old histogram which is caused by volume scatters.

According to Toh et al. [67], the scattering increased with age for all polarization in general for the L-band frequency. The L-band scattering coefficient showed the trend increasing with the age of oil palm more than 20 years. Besides that, according to Teng et al. [6], the scattering value for HH polarization using the L-band was increasing attenuation of waves propagating through to the soil surface and back, as the leaves, fronds, and trunks are growing larger.

The scattering value for each polarization (HH and HV) among the age of oil palm was increasing; according to Darmawan et al. [28], it was hypothesized that the growth of oil palms was caused by higher trunks, more leaves, more branches, and larger canopy followed by the condition of scattering value. In any case, the scatter values derived from the L-band are depending on wavelengths, polarization, incident angle, and temporal data; environments such as land moisture and landscape [25, 28, 68]; and the structure of oil palms such as size, geometry, and orientation of leaves, trunks, branches, and aerials or stilt roots [28, 68, 69].

4.2. Coefficient Determination of Scattering Model of Oil Palm Phenology.

The scatter model of oil palm phenology was performed separately for each radar wavelength (X-, C-, and L-band). In this study, the X-band showed the nonlinear oil palm phenology model in HH polarization with coefficient determination $R^2 = 0.65$, which means the model has moderate correlation. The C-band showed the nonlinear or quadratic model of oil palm phenology in VH polarization with coefficient determination $R^2 = 0.56$, which means the model

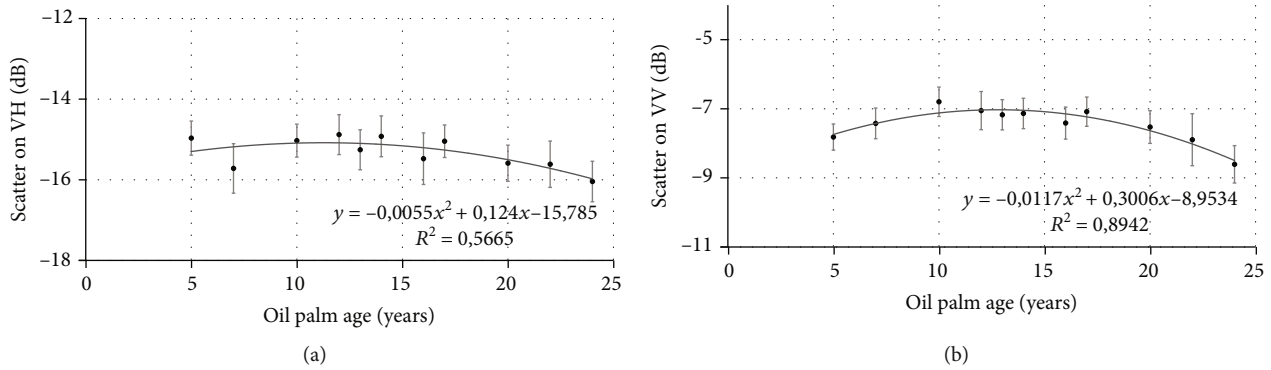


FIGURE 8: Scattering model of oil palm phenology on C-band with VH polarization (a) and VV polarization (b).

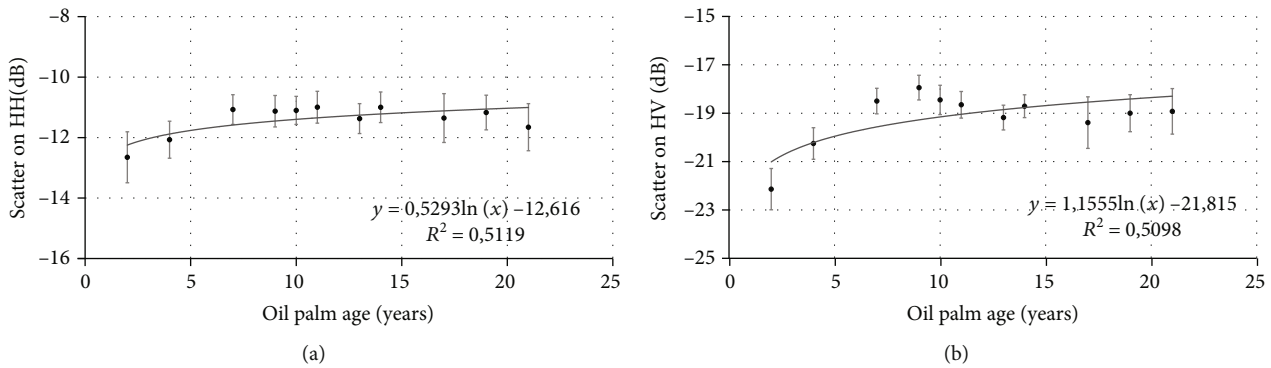


FIGURE 9: Scattering model of oil palm phenology on L-band with HH polarization (a) and HV polarization (b).

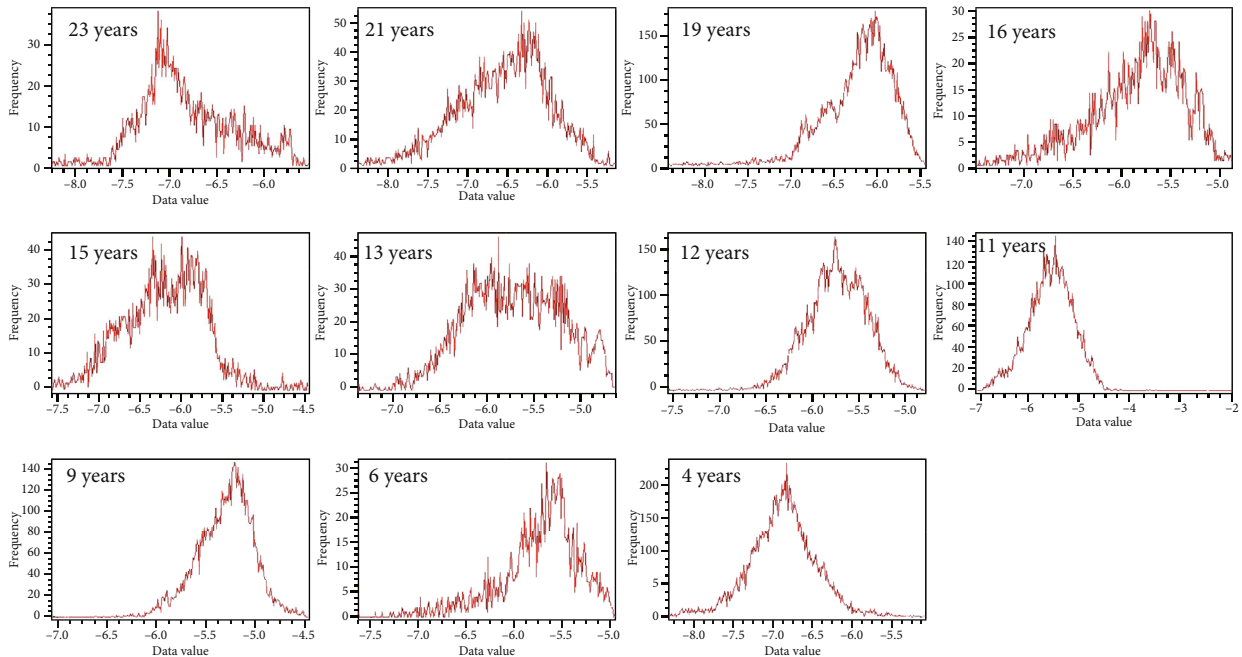


FIGURE 10: Histogram X-band for each age of oil palm.

has moderate correlation, and while on VV polarization with coefficient determination $R^2 = 0.89$, it means the model has strong correlation. The L-band showed the logarithmic model of oil palm phenology in HV polarization with coefficient determination $R^2 = 0.50$, which means the model has

moderate correlation, and while on HH polarization with coefficient determination $R^2 = 0.51$, it means the model has moderate correlation. In this case, the more potential of scattering model of oil palm phenology based on R^2 is using C-band on VV polarization.

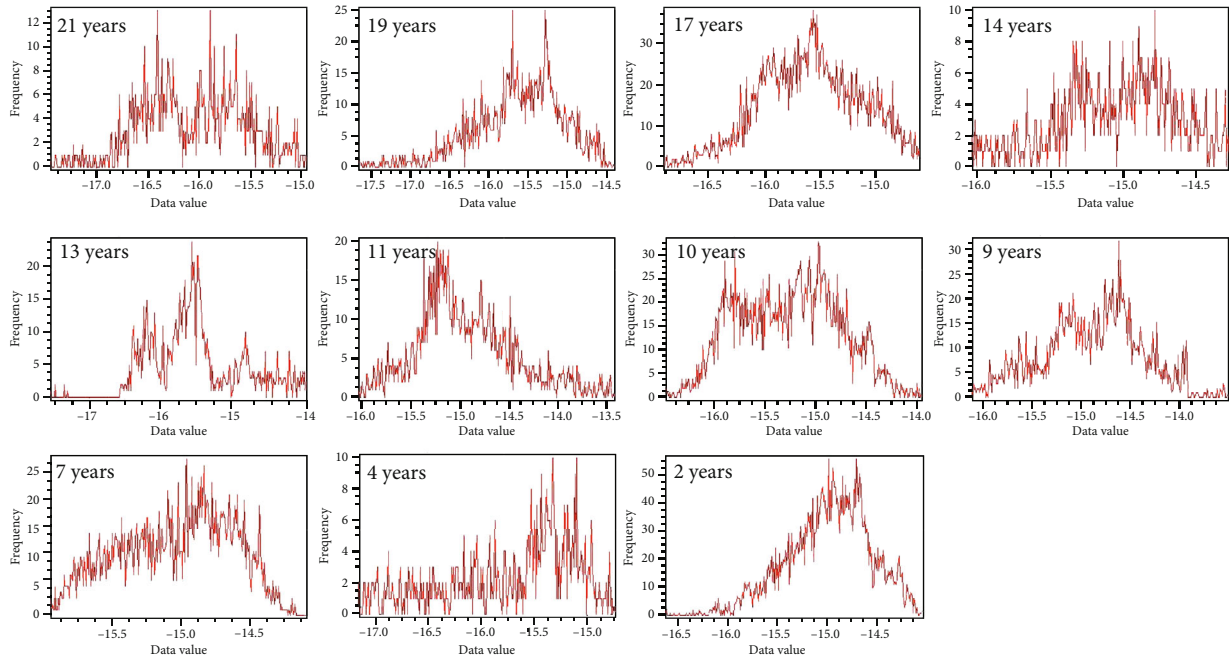


FIGURE 11: Histogram C-band on VH for each age of oil palm.

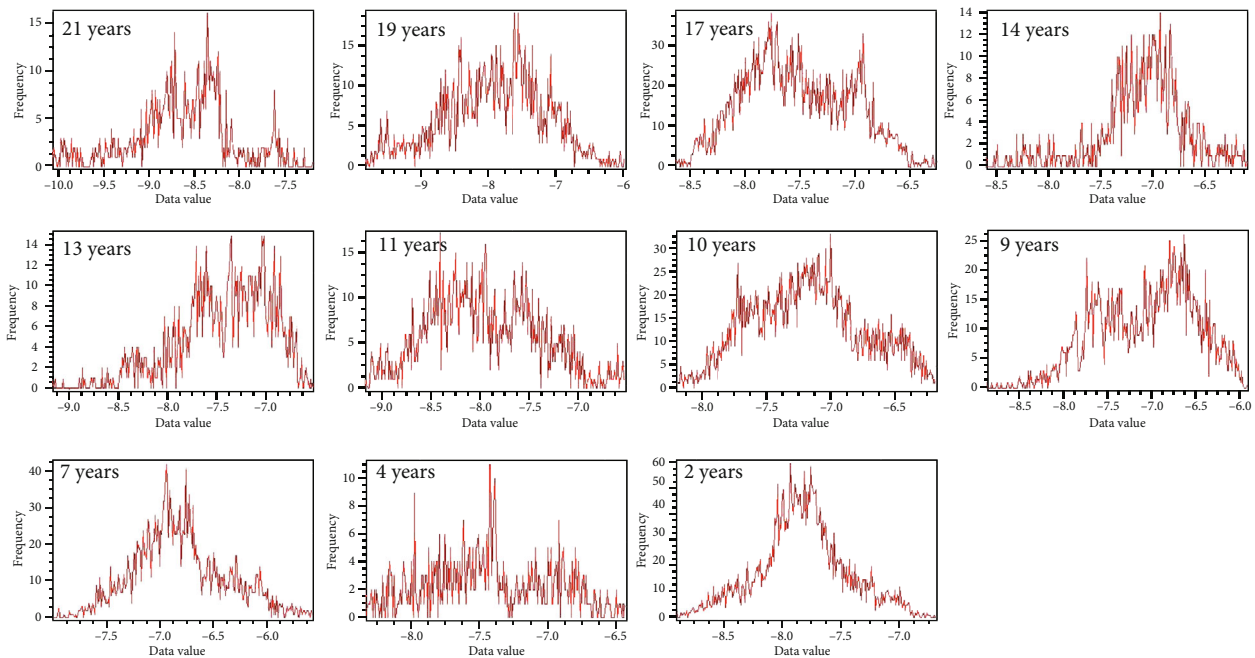


FIGURE 12: Histogram C-band on VV for each age of oil palm.

The scattering model with the moderate correlation also found by other researchers such as Tan et al. [10] has logarithmic regression for the correlating scattering value with oil palm age using ALOS PALSAR-2 with coefficient determination on HH polarization $R^2 = 0.49$, HV polarization with $R^2 = 0.27$, and ratio of HH/HV polarization with $R^2 = 0.26$, for study case in the southern part of peninsular Malaysia. Darmawan et al. [28] also used ALOS PALSAR-2 on HH and HV polarization having a logarithmic regression model with coefficient determination $R^2 = 0.62$ and

0.41 for study case area in Jerantut, Pahang, Malaysia. In other cases, Avtar et al. [70] for study area near Miri City, Sarawak, Malaysia, showed a logarithmic regression model for a variety of SAR data including TerraSAR-X (X-band) on HH polarization with coefficient determination $R^2 = 0.075$; Radarsat-2 (C-band) on HH, HV, and VV polarization with coefficient determination $R^2 = 0.39$, 0.49 , and 0.39 ; and ALOS PALSAR-2 (L-band) on HH and HV polarization with coefficient determination $R^2 = 0.62$ and 0.77 . Okarda et al. [32] studied the relationship between the age

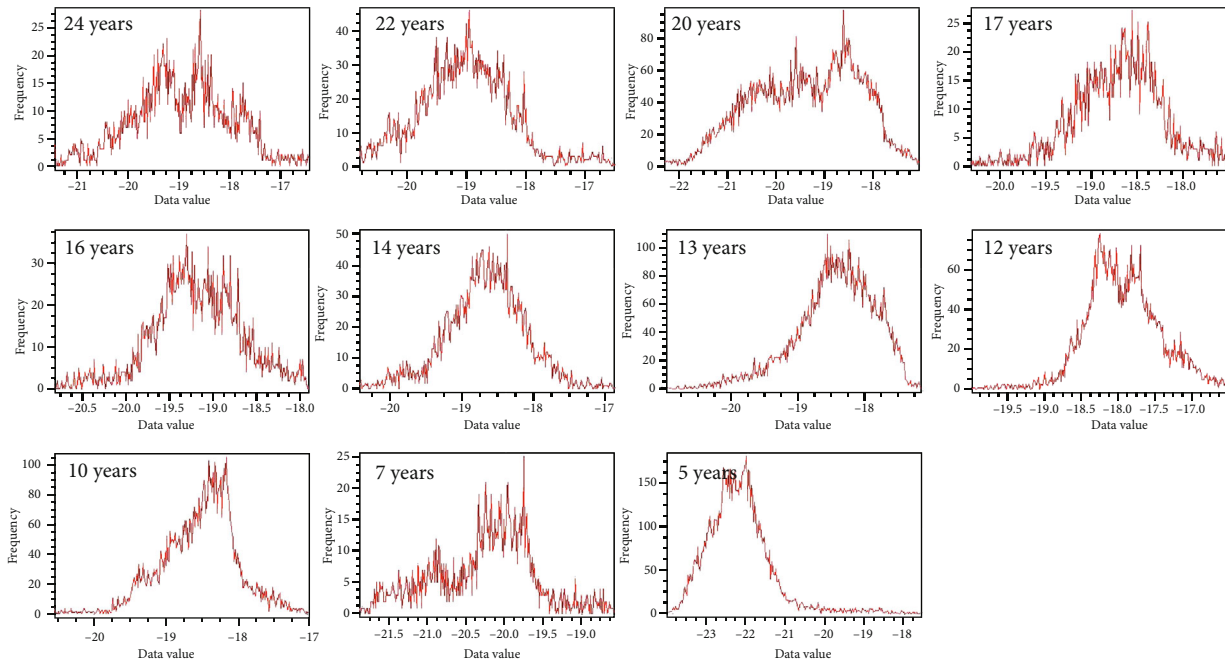


FIGURE 13: Histogram L-band on HV for each age of oil palm.

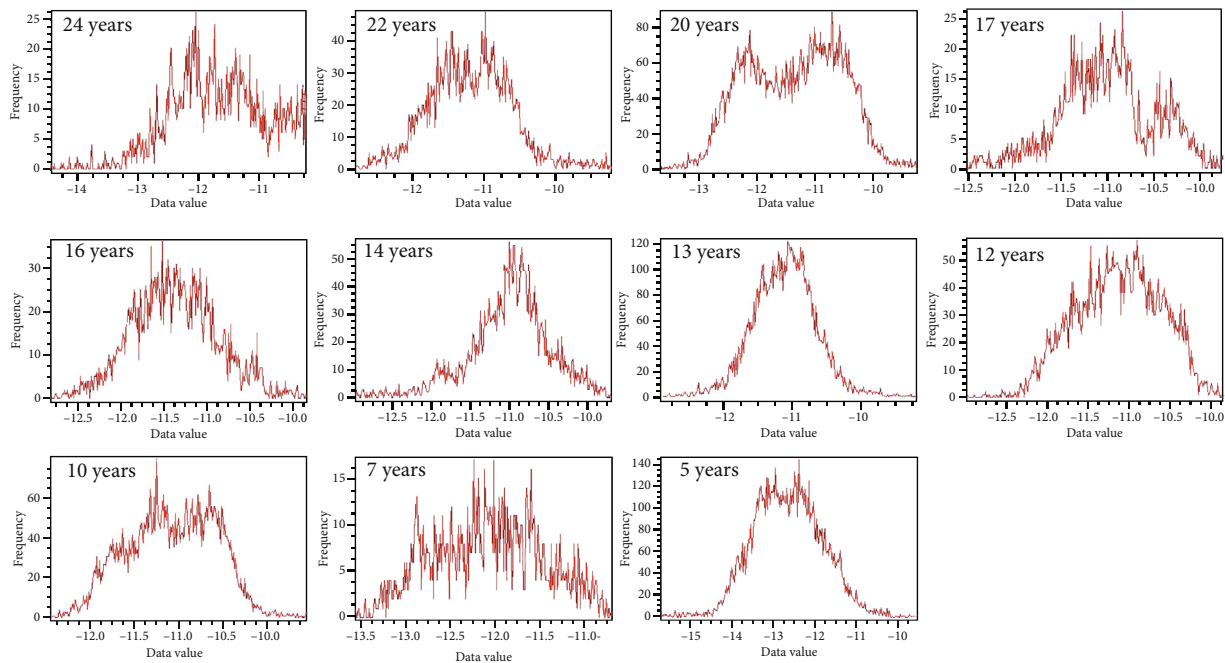


FIGURE 14: Histogram L-band on HH for each age of oil palm.

of oil palm in mineral soil and age and peatland in Central Kalimantan, Indonesia, using ALOS PALSAR-2 on HH and HV polarization. The scattering model has linear regression with coefficient determination on HH and HV between age and mineral soil with $R^2 = 0.55$ and 0.37 and age and peatland on HH and HV with $R^2 = 0.36$ and 0.28 . For C-band data, it was studied by Carolita et al. [15] using Sentinel-1A on HH and HV polarization. The scattering model has non-linear regression (quadratic model) with coefficient determi-

nation $R^2 = 0.68$ for HH and HV with $R^2 = 0.77$ for study case area in Asahan, North Sumatra Indonesia.

5. Conclusions

This study investigated the scattering model of oil palm phenology based on X-, C-, and L-band polarimetric SAR imaging in Asahan Regency, North Sumatra, Indonesia. We generated scattering values for different ranges of oil palm

age: 0-5, 5-10, 10-15, 15-20, and 20-25 years, with different scattering characteristics for each X-, C-, and L-band polarimetric SAR imaging depending on the wavelength and age ranges of oil palm. Finally, we found the scattering model of oil palm phenology based on the X-band on HH polarization which is $y = -0.0114x^2 + 0.2741x - 7.2823$ with $R^2 = 0.65$. The C-band on VH polarization is $y = -0.0055x^2 + 0.1248x - 15.785$ with $R^2 = 0.56$, while that on VV polarization is $y = -0.0117x^2 + 0.3006x - 8.9534$ with $R^2 = 0.89$. The L-band on HH polarization is $y = 0.5293 \ln(x) - 12.616$ with $R^2 = 0.51$, while that on HV polarization is $y = 1.1555 \ln(x) - 21.815$ with $R^2 = 0.50$. In this case, the more potential of the scattering model of oil palm phenology based on R^2 is using C-band on VV polarization. However, the scattering model can be used and applied to identify the phenology of oil palm in Indonesia, which is the main parameter in yield estimation, also required for the tax estimation, replanting time, and identification of oil palm diseases. The scattering model being developed needs to improve accuracy by integrating multisource-multispectral data, including different wavelengths on optical data and microwaves and more in situ data.

Data Availability

The data used to support the findings of this study are not yet available because other research work requiring data remains incomplete.

Conflicts of Interest

The authors declare no conflict of interest.

Acknowledgments

This research was funded by the Ministry of Research and Technology/National Research and Innovation (Kemenristek/BRIN) and Agency Indonesia Endowment Fund for Education (LPDP), with Contract No. 249/E1/PRN/2020. In addition, the researchers would like to thank Kemenristek/BRIN, LPDP, LAPAN, PPKS, and LPPM Itenas Bandung.

References

- [1] W. Li, H. Fu, L. Yu et al., "Stacked autoencoder-based deep learning for remote-sensing image classification: a case study of African land-cover mapping," *International Journal of Remote Sensing*, vol. 37, no. 23, pp. 5632–5646, 2016.
- [2] R. Dong, W. Li, H. Fu et al., "Oil palm plantation mapping from high-resolution remote sensing images using deep learning," *International Journal of Remote Sensing*, vol. 41, no. 5, pp. 2022–2046, 2020.
- [3] Y. Basiron, "Palm oil production through sustainable plantations," *European Journal of Lipid Science and Technology*, vol. 109, no. 4, pp. 289–295, 2007.
- [4] R. Hårdter, W. Y. Chow, and O. S. Hock, "Intensive plantation cropping, a source of sustainable food and energy production in the tropical rain forest areas in Southeast Asia," *Forest Ecology and Management*, vol. 91, no. 1, pp. 93–102, 1997.
- [5] D. Sheil, A. Casson, E. Meijaard et al., *Oil Palm Basics; What Do we Know and What Do we Need to Know?*, Center for International Forestry Research, 2009.
- [6] K. C. Teng, J. Y. Koay, S. H. Tey, K. S. Lim, H. T. Ewe, and H. T. Chuah, "A dense medium microwave backscattering model for the remote sensing of oil palm," *IEEE Transactions on Geoscience and Remote Sensing*, vol. 53, no. 6, pp. 3250–3259, 2015.
- [7] H. Aholoukpè, B. Dubos, A. Flori et al., "Estimating above-ground biomass of oil palm: Allometric equations for estimating frond biomass," *Forest Ecology and Management*, vol. 292, pp. 122–129, 2013.
- [8] E. Fitzherbert, M. Struebig, A. Morel et al., "How will oil palm expansion affect biodiversity?," *Trends in Ecology & Evolution*, vol. 23, no. 10, pp. 538–545, 2008.
- [9] K. L. Chong, K. D. Kanniah, C. Pohl, and K. P. Tan, "A review of remote sensing applications for oil palm studies," *Geo-Spatial Information Science*, vol. 20, no. 2, pp. 184–200, 2017.
- [10] K. P. Tan, K. D. Kanniah, and A. P. Cracknell, "Use of UK-DMC 2 and ALOS PALSAR for studying the age of oil palm trees in southern peninsular Malaysia," *International Journal of Remote Sensing*, vol. 34, no. 20, pp. 7424–7446, 2013.
- [11] R. H. Corley and P. B. Tinker, *The Oil Palm*, John Wiley & Sons, 2008.
- [12] R. H. V. Corley, *Oil Palm Physiology: A Review*, Incorporated Society of Planters, 1973.
- [13] G. Squire, "The Oil Palm. 4th Edition. Edited by R. H. V. Corley and P. B. Tinker. Oxford: Blackwell Publishing (2003), pp. 284, £115.00. ISBN 0-632-05212-0," *Experimental Agriculture*, vol. 41, no. 1, pp. 121–121, 2005.
- [14] H. Z. M. Shafri, N. Hamdan, and M. I. Sariapan, "Semi-automatic detection and counting of oil palm trees from high spatial resolution airborne imagery," *International Journal of Remote Sensing*, vol. 32, no. 8, pp. 2095–2115, 2011.
- [15] I. Carolita, S. Darmawan, R. Permana et al., "Comparison of optic Landsat-8 and SAR Sentinel-1 in oil palm monitoring, case study: Asahan, North Sumatera, Indonesia," *IOP Conference Series: Earth and Environmental Science*, vol. 280, 2019.
- [16] A. Chemura, I. van Duren, and L. M. van Leeuwen, "Determination of the age of oil palm from crown projection area detected from WorldView-2 multispectral remote sensing data: the case of Ejisu-Juaben district, Ghana," *ISPRS Journal of Photogrammetry and Remote Sensing*, vol. 100, pp. 118–127, 2015.
- [17] J. McMorro, "Linear regression modelling for the estimation of oil palm age from Landsat TM," *International Journal of Remote Sensing*, vol. 22, no. 12, pp. 2243–2264, 2010.
- [18] S. Darmawan, D. K. Sari, K. Wikantika, A. Tridawati, R. Hernawati, and M. K. Sedu, "Identification before-after forest fire and prediction of mangrove forest based on Markov-cellular automata in part of Sembilang national park, Banyuasin, South Sumatra, Indonesia," *Remote Sensing*, vol. 12, no. 22, pp. 3700–3725, 2020.
- [19] F. M. Henderson and A. J. Lewis, "Radar detection of wetland ecosystems: a review," *International Journal of Remote Sensing*, vol. 29, no. 20, pp. 5809–5835, 2008.
- [20] N. M. Yusoff, F. M. Muharam, W. Takeuchi, S. Darmawan, and M. H. Abd Razak, "Phenology and classification of abandoned agricultural land based on ALOS-1 and 2 PALSAR multi-temporal measurements," *International Journal of Digital Earth*, vol. 10, no. 2, pp. 155–174, 2017.

- [21] S. Darmawan, D. K. Sari, W. Takeuchi, K. Wikantika, and R. Hernawati, "Development of aboveground mangrove forests' biomass dataset for Southeast Asia based on ALOS-PALSAR 25-m mosaic," *Journal of Applied Remote Sensing*, vol. 13, no. 4, 2019.
- [22] S. Darmawan, I. Carolita, and E. Ananta, "Identification of oil palm plantation on multiscatter and resolution of SAR data using variety of classifications algorithm (case study: Asahan District, North Sumatera Province)," *In Proceedings of the IOP Conference Series: Earth and Environmental Science*, vol. 500, 2020.
- [23] B. Brisco, "Mapping and monitoring surface water and wetlands with synthetic aperture radar," in *Remote Sensing of Wetlands*, pp. 119–136, Natural Resources Canada, 2015.
- [24] N. E. Mohd Najib, K. D. Kanniah, A. P. Cracknell, and L. Yu, "Synergy of active and passive remote sensing data for effective mapping of oil palm plantation in Malaysia," *Forests*, vol. 11, no. 8, p. 858, 2020.
- [25] S. Darmawan, W. Takeuchi, Y. Vetrira, K. Wikantika, and D. K. Sari, "Impact of topography and tidal height on ALOS palsar polarimetric measurements to estimate aboveground biomass of mangrove forest in Indonesia," *Journal of Sensors*, vol. 2015, 13 pages, 2015.
- [26] Y. Qin, X. Xiao, J. Dong et al., "Mapping forests in monsoon Asia with ALOS PALSAR 50-m mosaic images and MODIS imagery in 2010," *Scientific Reports*, vol. 6, no. 1, pp. 1–10, 2016.
- [27] L. Nordin, "Application of Airsar data to oil palm tree," in *Proceedings of the Proceedings of the Asian Conference on Remote Sensing*, pp. 5–9, Kathmandu, India, 2002.
- [28] S. Darmawan, W. Takeuchi, A. Haryati, R. A. M. Najib, and M. Na'Aim, "An investigation of age and yield of fresh fruit bunches of oil palm based on ALOS PALSAR 2," *Proceedings of the IOP Conference Series: Earth and Environmental Science*, vol. 37, 2016.
- [29] I. Carolita, D. Yudhatama, D. Dirgahayu et al., "Silvia Informasi Spasial Tematik Klasifikasi Tanaman Sawit Berdasarkan Umur," in *Pusat Pemanfaatan Penginderaan Jauh*, LAPAN, Jakarta, 2019.
- [30] I. Carolita, J. Sitorus, J. Manalu, and D. Wiratmoko, "Growth profile analysis of oil palm by using spot 6 the case of North Sumatra," *International Journal of Remote Sensing and Earth Sciences (IJReSES)*, vol. 12, no. 1, p. 21, 2017.
- [31] J. Sitoms, P. Bidang, and P. Daia, "Pengembangan model estimasi umur tanaman sawit dengan menggunakan data landsat-Tm," *Jauh dan Pengolahan Data Citra Digital*, vol. 1, pp. 14–19, 2004.
- [32] B. Okarda, I. Carolita, T. Kartika, and H. Komarudin, "Mapping of smallholder oil palm plantation and development of a growth model," *Proceedings of the IOP Conference Series: Earth and Environmental Science*, vol. 169, 2018.
- [33] A. C. Crossland, S. A. Sinambela, A. S. Sitorus, and A. W. Sitorus, "The coastal zone of Asahan regency: an area of international importance for migratory waders in North Sumatra province, Indonesia," *Stilt*, vol. 55, pp. 8–12, 2009.
- [34] A. Ma, "Agro-pastoral and preservation of local wisdom Bondang for agricultural sustainability in Asahan, North Sumatra," *Agricultura*, vol. 105, pp. 110–113, 2018.
- [35] *The Recent Development of the Indonesian Palm Oil Industry | Indonesian Palm Oil Association (GAPKI IPOA)*, October 2020, <https://gapki.id/en/news/18397/the-recent-development-of-the-indonesian-palm-oil-industry>.
- [36] D. Rutz and R. Janssen, "Socio-economic impacts of bioenergy production," *Socio-Economic Impacts of Bioenergy Production*, pp. 1–297, 2014, 9783319038.
- [37] M. Masril, Nazaruddin, and J. Hidayati, "Improving the utilization of palm oil mill through fulfillment of fresh fruit bunch," *IOP Conference Series: Materials Science and Engineering*, vol. 801, 2020.
- [38] S. Budidarsono, A. Susanti, and A. Zoomers, "Oil palm plantations in Indonesia: the implications for migration, settlement/resettlement and local economic development," in *Biofuels - Economy, Environment and Sustainability*, pp. 173–193, 2013.
- [39] S. Gebhardt, J. Huth, L. D. Nguyen, A. Roth, and C. Kuenzer, "A comparison of TerraSAR-X Quadpol backscattering with RapidEye multispectral vegetation indices over rice fields in the Mekong Delta, Vietnam," *International Journal of Remote Sensing*, vol. 33, no. 24, pp. 7644–7661, 2012.
- [40] J. S. Lee, L. Jurkevich, P. Dewaele, P. Wambacq, and A. Oosterlinck, "Speckle filtering of synthetic aperture radar images: a review," *Remote Sensing Reviews*, vol. 8, no. 4, pp. 313–340, 1994.
- [41] H. Omar, M. Misman, and A. Kassim, "Synergetic of PALSAR-2 and sentinel-1A SAR polarimetry for retrieving aboveground biomass in dipterocarp forest of Malaysia," *Applied Sciences*, vol. 7, no. 7, p. 675, 2017.
- [42] J.-S. Lee, J.-H. Wen, T. L. Ainsworth, K.-S. Chen, and A. J. Chen, "Improved sigma filter for speckle filtering of SAR imagery," *IEEE Transactions on Geoscience and Remote Sensing*, vol. 47, no. 1, pp. 202–213, 2009.
- [43] J. Amini and J. T. Sri Sumantyo, "SAR and optical images for forest biomass estimation," *Biomass - Detection, Production and Usage*, Darko Matovic, Ed., pp. 53–74, 2011.
- [44] J. Hu, P. Ghamisi, and X. Zhu, "Feature extraction and selection of Sentinel-1 dual-pol data for global-scale local climate zone classification," *ISPRS International Journal of Geo-Information*, vol. 7, no. 9, p. 379, 2018.
- [45] R. Düring, F. N. Koudogbo, M. Weber, and I. Gmbh, "TerraSAR-X and TanDEM-X: Revolution in spaceborne radar," in *Proceedings of the The International Archives of The Photogrammetry, Remote Sensing and Spatial Information Sciences*, pp. 227–234, Beijing, 2008.
- [46] *Airbus Defence and Space, Radiometric Calibration of TerraSAR-X Data, Beta Naught and Sigma Naught Coefficient Calculation*, Innfoterra GMBH, Friedrichshafen, Germany, 2008.
- [47] C. B. Barber, D. P. Dobkin, and H. Huhdanpaa, "The Quickhull algorithm for convex hulls," *ACM Transactions on Mathematical Software*, vol. 22, no. 4, pp. 469–483, 1996.
- [48] Y. W. Kee, A. R. M. Shariff, A. M. Sood, and L. Nordin, "Application of SAR data for oil palm tree discrimination," *IOP Conference Series: Earth and Environmental Science*, vol. 169, 2018.
- [49] A. Schubert, N. Miranda, D. Geudtner, and D. Small, "Sentinel-1A/B combined product geolocation accuracy," *Remote Sensing*, vol. 9, no. 6, pp. 607–616, 2017.
- [50] F. Filipponi, "Sentinel-1 GRD preprocessing workflow," *Proceedings*, vol. 18, no. 1, p. 11, 2019.
- [51] M. Shimada, "Model-based polarimetric SAR calibration method using forest and surface-scattering targets," *IEEE Transactions on Geoscience and Remote Sensing*, vol. 49, no. 5, pp. 1712–1733, 2011.
- [52] T. F. Chan, G. H. Golub, and R. J. Leveque, "Statistical computing: algorithms for computing the sample variance: analysis

- and recommendations,” *American Statistician*, vol. 37, pp. 242–247, 1983.
- [53] A. S. Hess and J. R. Hess, “Linear regression and correlation,” *Transfusion*, vol. 57, no. 1, pp. 9–11, 2016.
- [54] J. P. Holcomb, N. R. Draper, H. Smith, J. O. Rawlings, S. G. Pantula, and D. A. Dickey, “Applied regression analysis applied regression analysis,” *A Research Tool*, vol. 53, 1999.
- [55] A. C. Cohen, “On estimating the mean and standard deviation of truncated normal distributions,” *Journal of the American Statistical Association*, vol. 44, no. 248, pp. 518–525, 1949.
- [56] P. Schober, C. Boer, and L. A. Schwarte, “Correlation coefficients: appropriate use and interpretation,” *Anesthesia & Analgesia*, vol. 126, no. 5, pp. 1763–1768, 2018.
- [57] A. I. Flores-Anderson, K. E. Herndon, R. B. Thapa et al., *THE SAR HANDBOOK: Comprehensive Methodologies for Forest Monitoring and Biomass Estimation*, SERVIR Global, Sparkman Drive, Huntsville, 2019.
- [58] J. van der Sanden, *Radar Remote Sensing to Support Tropical Forest Management*, Tropenbos-Guyana Programme and the Wageningen Agricultural University, 1997.
- [59] R. Bamler, “Principles of synthetic aperture radar,” *Surveys in Geophysics*, vol. 21, pp. 147–157, 2000.
- [60] J. J. Van Zyl and Y. Kim, *Synthetic Aperture Radar Polarimetry*, J. H. Yuen, Ed., A John Wiley and Sons, Inc., Publication, California, 2011.
- [61] S. Martinis and C. Rieke, “Backscatter analysis using multi-temporal and multi-frequency SAR data in the context of flood mapping at river Saale, Germany,” *Remote Sensing*, vol. 7, no. 6, pp. 7732–7752, 2015.
- [62] J. A. Richards, P. W. Woodgate, and A. K. Skidmore, “An explanation of enhanced radar backscattering from flooded forests,” *International Journal of Remote Sensing*, vol. 8, no. 7, pp. 1093–1100, 2007.
- [63] E.-M. Bernhard, A. Twele, and M. Gähler, “Brandflächendetektion auf Basis von X-band Radarsatellitendaten im Europäischen Mittelmeerraum,” *Photogrammetrie - Fernerkundung - Geoinformation*, vol. 2011, no. 4, pp. 261–270, 2011.
- [64] T. M. Lillesand and R. W. Kiefer, *Remote Sensing and Image Interpretation*, Wiley, 1979.
- [65] A. Rosenqvist, *Analysis of the Backscatter Characteristics of Rubber, Oil palm and Irrigated rice in Multi-band Polarimetric Synthetic Aperture Radar Imagery*, Institute of Industrial Science, University of Tokyo, Tokyo, Japan, 1997.
- [66] E. J. M. Rignot, C. L. Williams, J. Way, and L. A. Viereck, “Mapping of forest types in Alaskan boreal forests using SAR imagery,” *IEEE Transactions on Geoscience and Remote Sensing*, vol. 32, no. 5, pp. 1051–1059, 1994.
- [67] C. M. Toh, H. T. Ewe, S. H. Tey, and Y. H. Tay, “A study on oil palm remote sensing at L-band with dense medium microwave backscattering model,” *IEEE Transactions on Geoscience and Remote Sensing*, vol. 57, no. 10, pp. 8037–8047, 2019.
- [68] R. Lucas, J. Armston, R. Fairfax et al., “An evaluation of the ALOS PALSAR L-band backscatter—above ground biomass relationship Queensland, Australia: impacts of surface moisture condition and vegetation structure,” *IEEE Journal of Selected Topics in Applied Earth Observations and Remote Sensing*, vol. 3, no. 4, pp. 576–593, 2010.
- [69] A. C. Morel, S. S. Saatchi, Y. Malhi et al., “Estimating above-ground biomass in forest and oil palm plantation in Sabah, Malaysian Borneo using ALOS PALSAR data,” *Forest Ecology and Management*, vol. 262, no. 9, pp. 1786–1798, 2011.
- [70] R. Avtar, R. Ishii, H. Kobayashi, H. Fadaei, R. Suzuki, and S. Herath, “Efficiency of multi-frequency, multi-polarized SAR data to monitor growth stages of oil palm plants in Sarawak, Malaysia,” in *2013 IEEE International Geoscience and Remote Sensing Symposium - IGARSS*, pp. 2137–2140, Melbourne, VIC, Australia, 2013.